A Phenomenological Description of the Thermomechanical Coupling and the Rate-dependent Behavior of Shape Memory Alloys

PAULO CESAR C. MONTEIRO JR,[1] MARCELO A. SAVI,[2,*] THEODORO ANTOUN NETTO[1] AND PEDRO MANUEL C. L. PACHECO[3]

[1]*Universidade Federal do Rio de Janeiro, COPPE – Department of Ocean Engineering 21.945.970, Rio de Janeiro, P.O. Box 68.508, Brazil*

[2]*Universidade Federal do Rio de Janeiro, COPPE – Department of Mechanical Engineering, 21.941.972, Rio de Janeiro, P.O. Box 68.503, Brazil*

[3]*CEFET/RJ, Department of Mechanical Engineering, 20.271.110, Rio de Janeiro, Brazil*

ABSTRACT: Shape memory alloys (SMAs) present a rate-dependent behavior, which means that the thermomechanical response depends on the loading rate. Therefore, although martensitic transformation can be considered as a non-diffusive process, the phase transformation critical stresses are temperature dependent and, since heat transfer process is time dependent, it affects the thermomechanical behavior of SMAs. This article deals with the rate dependence of SMAs, proposing a 1D constitutive model to describe this effect. The proposed model is formulated within the framework of continuum mechanics and thermomechanical coupling terms of the energy equation are incorporated in the formulation in order to describe the rate-dependent behavior. Numerical simulations are carried out comparing results with experimental data available in literature for different loading rates and environmental media, presenting a close agreement. Afterwards, numerical tests are performed in order to evaluate the model capabilities showing that it is capable to capture the general thermomechanical behavior of SMAs.

Key Words: shape memory alloys, thermomechanical coupling, constitutive model, rate dependency.

INTRODUCTION

SHAPE memory alloys (SMAs) present complex thermomechanical behaviors related to different physical processes, such as pseudoelasticity, shape memory effect, which may be one-way (SME) or two-way (TWSME), and phase transformation due to temperature variation. Besides, there are more complicated phenomena that have significant influence over its overall thermomechanical behavior, for instance: plastic behavior, tension–compression asymmetry, plastic-phase transformation coupling, transformation-induced plasticity, and thermomechanical coupling, among others. The hysteretic response of SMAs is one of their essential characteristics being related to the martensitic phase transformation. The hysteresis loop may be observed either in stress–strain curves or in strain–temperature curves and, in brief, it is possible to say that the external hysteresis loop can be defined as the envelope of all internal hysteresis loops, usually denoted as subloops (Bo and Lagoudas, 1999).

The thermomechanical behavior of SMAs has been described by different mathematical models that capture the main aspects of these alloys. The macroscopic approach is interested on SMAs phenomenological features. Paiva and Savi (2006) present an overview of the main macroscopic models discussed in literature and just to mention some of the references cited there one could refer to: Tanaka and Nagaki (1982); Liang and Rogers (1990); Brinson (1993); Boyd and Lagoudas (1996); Fremond (1996); Auricchio et al. (1997); Bernardini and Pence (2002, 2005); Ziólkowski (2007). As it is well known, SMA devices present a rate-dependence characteristic, which means that the thermomechanical response depends on loading rate (Shaw and Kyriakides, 1995; Tobushi et al., 1998; Prahlad and Chopra, 2001, 2003; Iadicola and Shaw, 2004; Chang et al., 2006; Auricchio et al. 2006; Kadkhodaei et al., 2007; Thiebaud et al., 2007; Zhu and Zhang, 2007; Davis et al., 2008; Grabe and Bruhns, 2008; Yoon, 2008; Dayananda and Subba Rao, 2008; Heintze and Seelecke, 2008).

*Author to whom correspondence should be addressed.
E-mail: savi@mecanica.ufrj.br

1045-389X/09/14 1675–13 $10.00/0 DOI: 10.1177/1045389X09341199

The phase transformation critical stresses are temperature dependent and, since the heat transfer process is time dependent and occurs in a large time scale, the thermomechanical behavior of SMAs is affected by the thermomechanical coupling. Some authors point that this behavior exclusively results from the thermomechanical coupling effect associated with the latent heat due phase transformation (Shaw and Kyriakides, 1995; Auricchio et al., 2007). The thermomechanical coupling is related to an exothermic process that occurs during the phase transformation from austenite to martensite and also an endothermic process associated with the reverse transformation. Martensitic transformation can be considered as a non-diffusive process for many practical situations where martensitic transformation occurs at rates close to the speed of the material shear wave (Iadicola and Shaw, 2007).

This article deals with the rate dependency in SMAs proposing a constitutive model to describe this effect. This description is done by considering the thermomechanical coupling terms in the energy equation. A constitutive model that is capable to describe the main thermomechanical features of SMAs in a flexible way is of concern (Savi et al., 2002; Baêta-Neves et al., 2004; Paiva et al., 2005; Savi and Paiva, 2005). Basically, this 1D constitutive model considers different material properties to each phase and four macroscopic phases for the description of the SMA behavior. The model also considers the plastic strains and plastic-phase transformation coupling, which allows the description of the two-way shape memory effect. Moreover, tension–compression asymmetry is taken into account. The proposed model is formulated within the framework of continuum mechanics. Numerical simulations are carried establishing a comparison with experimental data available in literature for different loading rates and environmental media. Numerical results present a close agreement with experimental tests. Afterwards, numerical tests are performed in order to show the model capabilities. Different thermomechanical loadings are of concern, conducting tests in different temperatures, loading rates, and environmental media. Moreover, effects related to plasticity are analyzed for different situations.

MATHEMATICAL MODELING

The thermomechanical behavior of solids may be modeled in the framework of continuum mechanics. In order to introduce a general formulation, a brief review concerning first and second principles of thermodynamics is presented. The local form of the Clausius–Duhem inequality for the 1D case may be written as follows:

$$\sigma\dot{\varepsilon} - \rho(\dot{\psi} + s\dot{T}) - \frac{q}{T}\frac{\partial T}{\partial x} \geq 0 \tag{1}$$

where the dot means time derivative, ρ is the specific mass, Ψ is the Helmholtz free energy, s is the specific entropy, T is the temperature, σ is the uniaxial stress, ε is the total strain, q is the heat flux, and x represents the 1D spatial coordinate. As a first hypothesis concerning the constitutive modeling, it is assumed that the Helmholtz free energy density is a function of a finite set of variables:

$$\psi = \psi(\varepsilon, \varepsilon^i, T, V), \tag{2}$$

where ε^i is the inelastic strain and V represents a set of internal variables. Since

$$\dot{\psi} = \frac{\partial \psi}{\partial \varepsilon}\dot{\varepsilon} + \frac{\partial \psi}{\partial \varepsilon^i}\dot{\varepsilon}^i + \frac{\partial \psi}{\partial T}\dot{T} + \frac{\partial \psi}{\partial v}\dot{V}, \tag{3}$$

the Clausius–Duhem inequality may be rewritten as follows:

$$\left(\sigma - \rho\frac{\partial \psi}{\partial \varepsilon}\right)\dot{\varepsilon} - \rho\frac{\partial \psi}{\partial \varepsilon^i}\dot{\varepsilon}^i - \left(s + \rho\frac{\partial \psi}{\partial T}\right)\dot{T} - \rho\frac{\partial \psi}{\partial V}\dot{V} - \frac{q}{T}\frac{\partial T}{\partial x} \geq 0. \tag{4}$$

Motivated by the Clausius–Duhem inequality, the generalized standard material approach based on thermodynamical formalism establishes the following definitions of the thermodynamical forces (Lemaitre and Chaboche, 1990),

$$\sigma = \rho\frac{\partial \psi}{\partial \varepsilon}; \quad \sigma^i = \rho\frac{\partial \psi}{\partial \varepsilon^i}; \quad B = -\rho\frac{\partial \psi}{\partial V} \tag{5}$$

$$s = -\frac{\partial \psi}{\partial T}; \quad \xi = \frac{1}{T}\left(\frac{\partial T}{\partial x}\right). \tag{6}$$

In order to describe irreversible processes, complementary laws are defined from a pseudo-potential of dissipation that is a function of internal variables:

$$\varphi = \varphi(\varepsilon^i, V, q). \tag{7}$$

The thermodynamical formalism establishes that if this potential φ is a positive convex function that vanishes at the origin, the Clausius–Duhen inequality is automatically satisfied by defining the thermodynamics fluxes as follows (Lemaitre and Chaboche, 1990; Fremond, 1987, 1996):

$$\sigma^i = \frac{\partial \varphi}{\partial \dot{\varepsilon}^i}; \quad B = \frac{\partial \psi}{\partial \dot{V}} \quad \text{and} \quad \xi = -\frac{\partial \varphi}{\partial (q/T)}. \tag{8}$$

Alternatively, these thermodynamics fluxes may be obtained from the dual of the potential of dissipation $\varphi^*(\sigma^i, B, \xi)$ allowing the definitions:

$$\dot{\varepsilon}^i = \frac{\partial \varphi^*}{\partial \sigma^i}; \quad \dot{V} = \frac{\partial \varphi^*}{\partial B} \quad \text{and} \quad q/T = -\frac{\partial \varphi^*}{\partial \xi}. \tag{9}$$

At this point, it is necessary to establish the energy conservation equation given by the first law of thermodynamics:

$$\rho\dot{\psi} = \sigma\dot{\varepsilon} - \frac{\partial q}{\partial x} - \rho T\dot{s} - \rho\dot{T}s. \tag{10}$$

Since we are interested in a single point description, spatial variations are neglected and a convection boundary condition is assumed. Therefore, the first law of thermodynamics has the following form:

$$\rho c_p\dot{T} = -h(T - T_\infty) + \sigma\dot{\varepsilon}^i + B\dot{V} + T\left[\frac{\partial\sigma}{\partial T}(\dot{\varepsilon} - \dot{\varepsilon}^i) - \frac{\partial B}{\partial T}\dot{V}\right] \tag{11}$$

where c_p is the specific heat at constant pressure, h is the convection coefficient, T_∞ is the environmental temperature. The first term on the equation right side is the convection term whereas the others are associated with the thermomechanical coupling.

CONSTITUTIVE MODEL

There are different ways to describe the thermomechanical behavior of SMAs (Paiva and Savi, 2006). Here, a constitutive model that is built upon the Fremond's model and previously addressed in different references (Savi et al., 2002; Baêta-Neves et al., 2004; Paiva et al., 2005; Savi and Paiva, 2005) is employed. This model considers different material properties for the description of the SMA behavior. The tension–compression asymmetry, the plasticity and the plastic-phase transformation coupling are incorporated in the model. The thermomechanical coupling is of concern and the continuum mechanics framework, briefly presented in the previous section, is employed to obtain the general constitutive equations. Four macroscopic phases are assumed: austenite A, twinned martensite M positive detwinned martensite M^+, and negative detwinned martensite M^-. Here, besides elastic strain ε^e and temperature T, plastic behavior is treated by assuming variables related to isotropic and kinematics hardening, respectively, γ and μ. These variables come from classical plasticity representing the way of how plastic strains modify the yield surface. Under these assumptions, the Helmholtz free energy density of each isolated phase is given by:

$$M^+:\ \rho\psi_1(\varepsilon^e, T, \gamma, \mu) = \frac{1}{2}E_M(\varepsilon^e)^2 - \alpha^T\varepsilon^e - \Gamma_1 - \Omega_M(T - T_0)\varepsilon^e + \frac{1}{2}K_M\gamma^2 + \frac{1}{2H_M}\mu^2 \tag{12}$$

$$M^-:\ \rho\psi_2(\varepsilon^e, T, \gamma, \mu) = \frac{1}{2}E_M(\varepsilon^e)^2 + \alpha^C\varepsilon^e - \Gamma_2 - \Omega_M(T - T_0)\varepsilon^e + \frac{1}{2}K_M\gamma^2 + \frac{1}{2H_M}\mu^2 \tag{13}$$

$$A:\ \rho\psi_3(\varepsilon^e, T, \gamma, \mu) = \frac{1}{2}E_A(\varepsilon^e)^2 - \Gamma_3 - \Omega_A(T - T_0)\varepsilon^e + \frac{1}{2}K_A\gamma^2 + \frac{1}{2H_A}\mu^2 \tag{14}$$

$$M:\ \rho\psi_4(\varepsilon^e, T, \gamma, \mu) = \frac{1}{2}E_M(\varepsilon^e)^2 - \Gamma_4 - \Omega_M(T - T_0)\varepsilon^e + \frac{1}{2}K_M\gamma^2 + \frac{1}{2H_M}\mu^2 \tag{15}$$

These functions consider the following material parameters, where subscript A is assumed for austenitic phase while M is used for martensitic phase: E is the elastic modulus, Ω is related to thermal expansion coefficient, K is the isotropic hardening parameter, and H is the kinematics hardening parameter; T_0 is a reference temperature, a^T and a^C are related to the stress–strain hysteresis loop size. Finally, Λ is a temperature-dependent function.

Now, it is possible to define the mixture free energy density, defining volume fractions for each phase: β_1 and β_2 are respectively, the positive M^+ and negative M^- detwinned martensite, β_3 is associated with austenitic phase A and β_4 is related to twinned martensite M. Since $\beta_4 = 1 - \beta_1 - \beta_2 - \beta_3$ it is possible to write an equation with only three volume fractions as follows:

$$\psi(\varepsilon^e, T, \gamma, \mu, \beta_1, \beta_2, \beta_3) = \sum_{n=1}^{3}\beta_n\psi_n + J_\Pi \tag{16}$$

where $J_\Pi = J_\Pi(\beta_1, \beta_2, \beta_3)$ is the indicator function related to the convex set Π, associated with the phase coexistence, that has the following form:

$$\Pi = \{\beta_n \in \mathbb{R} | 0 \le 1 (n = 1, 2, 3);\ \ \beta_1 + \beta_2 + \beta_3 = 1\}. \tag{17}$$

By assuming an additive decomposition $\varepsilon^e = \varepsilon - \varepsilon^p - \alpha_h^T\beta_1 + \alpha_h^C\beta_2$ where ε^p is the plastic strain, α_h^T and α_h^C are related to the horizontal size of the stress–strain hysteresis loop. Therefore, the free energy density can be written in an expanded form:

$$\begin{aligned}\psi(\varepsilon, \varepsilon^p, T, \gamma, \mu, \beta_1, \beta_2, \beta_3) &= -\left[\alpha^T\left(\varepsilon - \varepsilon^p - \alpha_h^T\beta_1 + \alpha_h^C\beta_2\right) - \Lambda_1\right]\beta_1 \\ &+ \left[\alpha^C\left(\varepsilon - \varepsilon^p - \alpha_h^T\beta_1 + \alpha_h^C\beta_2\right) - \Lambda_2\right]\beta_2 \\ &+ \frac{1}{2}E\left(\varepsilon - \varepsilon^p - \alpha_h^T\beta_1 + \alpha_h^C\beta_2\right)^2 \\ &- \Omega_A(T - T_0)(\varepsilon - \varepsilon^p - \alpha_h^T\beta_1 + \alpha_h^C\beta_2) \\ &+ \frac{1}{2}K_A\gamma^2 + \frac{1}{2H_A}\mu^2 - \Lambda_3\beta_3 + \Gamma_4 + J_\Pi\end{aligned} \tag{18}$$

It should be noticed that the material parameters of the mixture is defined by a rule of mixtures with the following form:

$$E = E_{\mathrm{M}} + (E_{\mathrm{A}} - E_{\mathrm{M}})\beta_3, \quad \Omega = \Omega_{\mathrm{M}} + (\Omega_{\mathrm{A}} - \Omega_{\mathrm{M}})\beta_3 \tag{19}$$

$$K = K_{\mathrm{M}} + (K_{\mathrm{A}} - K_{\mathrm{M}})\beta_3, \quad \frac{1}{H} = \frac{1}{H_{\mathrm{M}}} + \left(\frac{1}{H_{\mathrm{A}}} - \frac{1}{H_{\mathrm{M}}}\right)\beta_3 \tag{20}$$

Moreover, temperature-dependent functions are assumed, given by:

$$\Lambda_1 = \Gamma_4 - \Gamma_1 = \begin{cases} -L_0^T + \frac{L^T}{T_{\mathrm{M}}}(T - T_{\mathrm{M}}), & \text{if } T > T_{\mathrm{M}} \\ -L_0^T & \text{if } T \le T_{\mathrm{M}} \end{cases} \tag{21}$$

$$\Lambda_2 = \Gamma_4 - \Gamma_2 = \begin{cases} -L_0^C + \frac{L^C}{T_{\mathrm{M}}}(T - T_{\mathrm{M}}), & \text{if } T > T_{\mathrm{M}} \\ -L_0^C & \text{if } T \le T_{\mathrm{M}} \end{cases} \tag{22}$$

$$\Lambda_3 = \Gamma_4 - \Gamma_3 = \begin{cases} -L_0^A + \frac{L^A}{T_{\mathrm{M}}}(T - T_{\mathrm{M}}), & \text{if } T > T_{\mathrm{M}} \\ -L_0^A & \text{if } T \le T_{\mathrm{M}} \end{cases} \tag{23}$$

At this point, the definitions discussed in the previous sections are employed, and the thermodynamical forces are obtained:

$$\sigma = \rho\frac{\partial\psi}{\partial\varepsilon} = E(\varepsilon - \varepsilon^p) - \left(E\alpha^T + \alpha_h^T\right)\beta_1 + \left(E\alpha^C + \alpha_h^C\right)\beta_2 - \Omega(T - T_0) \tag{24}$$

$$\begin{aligned} B_1 \in -\rho\partial_1\psi = {} & \alpha^T(\varepsilon - \varepsilon^p) + \Lambda_1 \\ & - \left[2\alpha_h^T\alpha^T + E\left(\alpha_h^T\right)^2\right]\beta_1 \\ & + \left(\alpha_h^C\alpha^T + \alpha_h^T\alpha^C + E\alpha_h^T\alpha_h^C\right)\beta_2 + \alpha_h^T[E(\varepsilon - \varepsilon^p) \\ & - \Omega(T - T_0)] - \partial_1 J_\Pi \end{aligned} \tag{25}$$

$$\begin{aligned} B_2 \in -\rho\partial_2\psi = {} & -\alpha^C(\varepsilon - \varepsilon^p) + \Lambda_2 \\ & + \left(\alpha_h^T\alpha^C + \alpha_h^C\alpha^T + E\alpha_h^C\alpha_h^T\right)\beta_1 \\ & - \left[2\alpha_h^C\alpha^C + E\left(\alpha_h^C\right)^2\right]\beta_2 \\ & - \alpha_h^C[E(\varepsilon - \varepsilon^p) - \Omega(T - T_0)] - \partial_2 J_\Pi \end{aligned} \tag{26}$$

$$\begin{aligned} B_3 \in -\rho\partial_3\psi = {} & -\frac{1}{2}(E_{\mathrm{A}} - E_{\mathrm{M}}) \\ & \left(\varepsilon - \varepsilon^p - \alpha_h^T\beta_1 + \alpha_h^C\beta_2\right)^2 \\ & + \Lambda_3 + (\Omega_{\mathrm{A}} - \Omega_{\mathrm{M}})(T - T_0)(\varepsilon - \varepsilon^p - \alpha_h^T\beta_1 + \alpha_h^C\beta_2) \\ & - \frac{1}{2}(K_{\mathrm{A}} - K_{\mathrm{M}})\gamma^2 + \left(\frac{1}{2H_{\mathrm{A}}} - \frac{1}{H_{\mathrm{M}}}\right)\mu^2 - \partial_3 J_\Pi \end{aligned} \tag{27}$$

$$Y = -\rho\frac{\partial\psi}{\partial\gamma} = -K\gamma \tag{28}$$

$$Z = -\rho\frac{\partial\psi}{\partial\mu} = -\frac{1}{H}\mu \tag{29}$$

where $\partial_k (k = 1, 2, 3)$ are sub-differentials of the indicator function J_Π with respect to volume fraction (Rockafellar, 1970).

The dissipation process is governed by complementary laws where definition may be associated with the dual of the potential of dissipation defined as follows:

$$\begin{aligned} \varphi^* = {} & \frac{1}{2\eta_1}(B_1 + \eta_{ci}Y + \eta_{ck}Z)^2 + \frac{1}{2\eta_2}(B_2 + \eta_{ci}Y + \eta_{ck}Z)^2 \\ & + \frac{1}{2\eta_3}(B_3 + \eta_{ci}Y + \eta_{ck}Z)^2 + \frac{q}{T}\frac{\partial T}{\partial x} + J_f + J_\chi \end{aligned} \tag{30}$$

At this point, it should be highlighted that the form of this pseudo-potential establishes a coupling between thermodynamical forces related to phase transformation, B_i $(i = 1, 2, 3)$, and plasticity, represented by Y and Z. This means that the phase transformation may change plastic yield surface and vice-versa. Under this assumption, η_{ci} represents a parameter responsible for the isotropic hardening coupling while η_{ck} represents the kinematics hardening coupling. This kind of coupling is responsible for the description of the TWSME and the reader can find a more detailed discussion in Paiva et al. (2005) and Savi et al. (2002). Moreover, parameters η_1, η_2, and η_3 represent the internal dissipation related to the phase transformation and $J_\chi = J_\chi(\beta_1, \beta_2, \beta_3, \dot\beta_1, \dot\beta_2, \dot\beta_3)$ is the indicator function of the convex set χ used to describe subloops due to incomplete phase transformation and also to avoid improper transformations among martensitic variants ($\mathrm{M}^+ \to \mathrm{M}$ and $\mathrm{M}^- \to \mathrm{M}$ for instance).

$$\chi = \left\{ \dot\beta_k \in \mathbb{R} \,\middle|\, \begin{matrix} \dot\varepsilon\dot\beta_1 \ge 0 \ \text{ and } \ \dot\varepsilon\dot\beta_3 \le 0 \ \text{ if } \varepsilon_0 > 0 \\ \dot\varepsilon\dot\beta_2 \le 0 \ \text{ and } \ \dot\varepsilon\dot\beta_3 \ge 0 \ \text{ if } \varepsilon_0 < 0 \end{matrix} \right\} \tag{31}$$

for $\dot\sigma \neq 0$, where $\varepsilon_0 = \varepsilon - \Omega(T - T_0)/E$. On the other hand, for $\dot\sigma = 0$,

$$pt\chi = \left\{ \dot\beta_k \in \mathbb{R} \,\middle|\, \begin{matrix} \left|\dot T\dot\beta_1\right| < 0 \ \text{ if } T > 0, \ \underset{=0 \text{ otherwise}}{\sigma < \sigma_{\mathrm{M}}^{Crit}} \ \text{ and } \ \beta_1^S = 0 \\ \left|\dot T\dot\beta_2\right| < 0 \ \text{ if } T > 0, \ \underset{=0 \text{ otherwise}}{\sigma < \sigma_{\mathrm{M}}^{Crit}} \ \text{ and } \ \beta_2^S = 0 \\ \dot T\dot\beta_3 \ge 0 \\ -\dot\beta_1^2 - \dot\beta_1\dot\beta_3 = 0 \ \text{ or } -\dot\beta_2^2 - \dot\beta_2\dot\beta_3 = 0 \end{matrix} \right\} \tag{32}$$

In the χ set, β_1^S and β_2^S represent the volume fraction of detwinned martensite in the beginning of phase transformation and σ_M^{Crit} is the critical stress. J_f is the function associated with the yield surface, defined as follows:

$$f(X, Y, Z) = |X + HZ| - (\sigma_Y - Y) \tag{33a}$$

Or alternatively,

$$f(\sigma, \mu, \gamma) = |\sigma + \mu| - (\sigma_Y - K\gamma) \tag{33b}$$

Therefore, the thermodynamics fluxes are given by:

$$\dot{\beta}_1 \in \partial_{B_1}\varphi^* = \frac{1}{\eta_1}(B_1 + \eta_{ci}Y + \eta_{ck}Z) \tag{34}$$

$$\dot{\beta}_2 \in \partial_{B_2}\varphi^* = \frac{1}{\eta_2}(B_2 + \eta_{ci}Y + \eta_{ck}Z) \tag{35}$$

$$\dot{\beta}_3 \in \partial_{B_3}\varphi^* = \frac{1}{\eta_3}(B_3 + \eta_{ci}Y + \eta_{ck}Z) \tag{36}$$

$$\dot{\varepsilon}^p \in \partial_X\varphi^* = \lambda\frac{(X + HZ)}{|X + HZ|} \tag{37}$$

$$\dot{\gamma} \in \partial_Y\varphi^* = \lambda + \eta_{ci}(\dot{\beta}_1 + \dot{\beta}_2 - \dot{\beta}_3) \tag{38}$$

$$\dot{\mu} \in \partial_Z\varphi^* = \lambda H\frac{(X + HZ)}{|X + HZ|} + \eta_{ck}(\dot{\beta}_1 + \dot{\beta}_2 - \dot{\beta}_3). \tag{39}$$

Once again, it should be highlighted that there is a coupling between plastic and phase transformation behaviors. At this moment, there is a set of constitutive equations that describes the thermomechanical 1D behavior of SMAs:

$$\begin{aligned}\sigma = {} & E(\varepsilon - \varepsilon^p) - (E\alpha^T + \alpha_h^T)\beta_1 \\ & + (E\alpha^C + \alpha_h^C)\beta_2 - \Omega(T - T_0);\end{aligned} \tag{40}$$

$$\begin{aligned}\eta_1\dot{\beta}_1 = {} & \alpha^T(\varepsilon - \varepsilon^p) + \Lambda_1 - \left[2\alpha_h^T\alpha^T + E\left(\alpha_h^T\right)^2\right]\beta_1 \\ & + \left(\alpha_h^C\alpha^T + \alpha_h^T\alpha^C + E\alpha_h^T\alpha_h^C\right)\beta_2 + \alpha_h^T[E(\varepsilon - \varepsilon^p) - \Omega(T - T_0)] \\ & + \eta_{ci}K\gamma + \eta_{ck}\frac{1}{H}\mu - \partial_1 J_\Pi + \eta_1\partial_1 J_\chi\end{aligned} \tag{41}$$

$$\begin{aligned}\eta_2\dot{\beta}_2 = {} & -\alpha^C(\varepsilon - \varepsilon^p) + \Lambda_2 \\ & + \left(\alpha_h^T\alpha^C + \alpha_h^C\alpha^T + E\alpha_h^C\alpha_h^T\right)\beta_1 \\ & - \left[2\alpha_h^C\alpha^C + E\left(\alpha_h^C\right)^2\right]\beta_2 - \alpha_h^C[E(\varepsilon - \varepsilon^p) - \Omega(T - T_0)] \\ & + \eta_{ci}K\gamma + \eta_{ck}\frac{1}{H}\mu - \partial_2 J_\Pi + \eta_2\partial_2 J_\chi\end{aligned} \tag{42}$$

$$\begin{aligned}\eta_3\dot{\beta}_3 = {} & -\frac{1}{2}(E_A - E_M)\left(\varepsilon - \varepsilon^p - \alpha_h^T\beta_1 + \alpha_h^C\beta_2\right)^2 + \Lambda_3 \\ & + (\Omega_A - \Omega_M)(T - T_0)\left(\varepsilon - \varepsilon^p - \alpha_h^T\beta_1 + \alpha_h^C\beta_2\right) \\ & - \frac{1}{2}(K_A - K_M)\gamma^2 + \left(\frac{1}{2H_A} - \frac{1}{H_M}\right)\mu^2 \\ & + \eta_{ci}K\gamma + \eta_{ck}\frac{1}{H}\mu - \partial_3 J_\Pi + \eta_3\partial_3 J_\chi\end{aligned} \tag{43}$$

$$\dot{\varepsilon}^p = \lambda\frac{(\sigma - \mu)}{|\sigma - \mu|} \tag{44}$$

$$\dot{\gamma} = |\dot{\varepsilon}^p| + \eta_{ci}(\dot{\beta}_1 + \dot{\beta}_2 - \dot{\beta}_3) \tag{45}$$

$$\dot{\mu} = H|\dot{\varepsilon}^p| + \eta_{ck}(\dot{\beta}_1 + \dot{\beta}_2 - \dot{\beta}_3) \tag{46}$$

In order to contemplate different aspects of phase transformation kinetics, parameter $\eta_i (i = 1, 2, 3)$ may assume different values for cases of loading or unloading behaviors:

$$\begin{cases}\eta_i = \eta_i^L & \text{if } \dot{\varepsilon} \geq 0 \\ \eta_i = \eta_i^U & \text{if } \dot{\varepsilon} < 0\end{cases} \tag{47}$$

Moreover, in order to establish a temperature dependence of the yield limit, the following expression is considered:

$$\begin{cases}\sigma_Y = \sigma_Y^M & \text{if } T \leq T_M \\ \sigma_Y = \frac{\sigma_Y^M(T_A - T) + \sigma_Y^{A,i}(T - T_M)}{T_A - T_M} & \text{if } T_M \leq T \leq T_A \\ \sigma_Y = \frac{\sigma_Y^{A,i}(T_F - T) + \sigma_Y^{A,i}(T - T_A)}{T_F - T_A} & \text{if } T_A \leq T \leq T_F\end{cases} \tag{48}$$

where T_F is used to determine the angular coefficient of this linear interpolation.

The temperature variation is described by the energy equation that incorporates thermomechanical coupling terms as follows:

$$\begin{aligned}\rho c_p\dot{T} = {} & hA(T - T_\infty) + \sigma\dot{\varepsilon}^p + B_1\dot{\beta}_1 + B_2\dot{\beta}_2 \\ & + B_3\dot{\beta}_3 + Y\dot{\gamma} + Z\dot{\mu} \\ & + T\left[\frac{\partial\sigma}{\partial T}(\dot{\varepsilon} - \dot{\varepsilon}^p) - \frac{\partial B_1}{\partial T}\dot{\beta}_1 - \frac{\partial B_2}{\partial T}\dot{\beta}_2 - \frac{\partial B_3}{\partial T}\dot{\beta}_3 - \frac{\partial Y}{\partial T}\dot{\gamma} - \frac{\partial Z}{\partial T}\dot{\mu}\right]\end{aligned} \tag{49}$$

NUMERICAL SIMULATIONS

In order to evaluate the model capability to describe the thermomechanical coupling of SMAs, a numerical procedure developed by Savi et al. (2002) and Paiva et al. (2005) is employed to deal with the non-linearities in the formulation. Basically, the procedure employs an operator split technique together with an iterative process, using a projection algorithm to

treat the sub-differentials. By using this procedure, numerical simulations are carried out for different physical situations. Thermal problem is treated by considering any classical integration scheme as Euler or Runge–Kutta method. Both approaches are tested presenting similar results.

An important aspect concerning the numerical simulation is the convection coefficient, h. A procedure is employed in order to obtain a temperature-dependent coefficient, here presented for vertical cylinders (Incropera and Dewitt, 2001):

$$h = \frac{kNu}{l} \tag{50}$$

where k is the heat conduction coefficient and Nu is the Nusselt number defined as follows:

$$Nu^{1/2} = 0.825 + \frac{0.387 Ra_L^{1/2}}{[1 + (0.492/1Pr)^{9/16}]^{8/27}} \quad \text{for } 10^{-1} < Ra_i < 10^{12} \tag{51}$$

and Ra is the Rayleigh number given by:

$$Ra_l = \frac{g\omega(T - T_\infty)l^3}{\nu\zeta} \tag{52}$$

where g is the acceleration of gravity, ω is the thermal expansion coefficient, T is the body temperature, T_∞ is the oncoming fluid temperature, l is length of cylinder, ν is the kinematic viscosity, and ζ is the thermal diffusivity. Note that the subscript designates the length on which it is based.

Figure 1 presents simulation results for an SMA wire of 0.03 mm diameter (w1) and an SMA wire of 0.6 mm diameter (w2) subjected to natural convection considering a temperature dependent (updated h) and a constant convection coefficient (average h). Results for both approaches are in close agreement with experimental tests obtained by Prahlad and Chopra (2003).

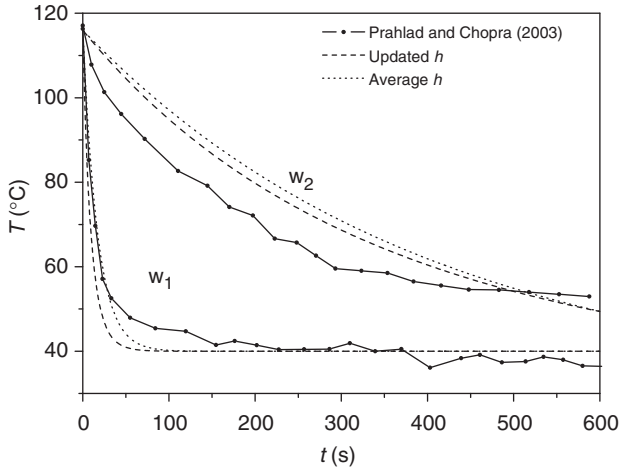

Figure 1. *Comparative results between an SMA wire (w1) and (w2) cooling under natural convection.*

At this point, let us consider a verification of the model comparing numerical results with those obtained from experimental analysis presented by Shaw and Kyriakides (1995). These experimental tests consider NiTi wires of 1.07 mm diameter and subjected to different loading rates at distinct temperatures and different media. The proposed model matches the experimental data by assuming model parameters presented in Table 1. Plastic parameters are omitted since this behavior is not in focus at this moment. Tension–compression asymmetry is also neglected in this analysis assuming $\alpha^T = \alpha^C = \alpha$ and $\alpha_h^T = \alpha_h^C = \alpha_h$, $L^T = L^C = L$, $L_0^T = L_0^C = L_0$, and $\eta_1 = \eta_2 = \eta$. The model verification considers a tensile test at environmental temperature $T_\infty = 70°\text{C}$ and three different loading rates $\dot{\varepsilon} = 0.04\,\text{s}^{-1}$ (Figure 2), $\dot{\varepsilon} = 0.004\,\text{s}^{-1}$ (Figure 3), $\dot{\varepsilon} = 0.0004\,\text{s}^{-1}$ (Figure 4). Figures 2–4 present the stress–strain curves together with the temperature evolution of tests performed with air as an environmental medium. Note that the thermomechanical coupling causes a temperature increase during austenite–martensite phase transformation and a temperature decrease during reverse transformation. This behavior affects the stress–strain curves that present a hysteresis loop reduction for faster loading rates.

Similar tests are now performed by assuming water as an environmental medium. Once again, numerical and experimental data are in close agreement. Since the water as an environmental medium causes a better balance between the thermomechanical coupling and the heat convection, it is noticeable that these tests are related to low temperature variations when compared with those in air medium (Figures 5–7).

The balance between heat generation due to phase transformations and convection may be better understood by considering tests with different, constants, values of the convection coefficient, h, with a loading rate $\dot{\varepsilon} = 0.04\,\text{s}^{-1}$. Figure 8 presents stress–strain curves

Table 1. Model thermomechanical properties (Shaw and Kyriakides, 1995).

Material properties				
E_A (GPa)	E_M (GPa)	α (MPa)	α_h	L_0 (MPa)
67	25	120	0.0335	1
L (MPa)	L_0^A (MPa)	L^A (MPa)	Ω_A (MPa/K)	Ω_M (MPa/K)
1	0.1	90	0.74	0.17
η^L (MPa s)	η^U (MPa s)	η_3^L (MPa s)	η_3^U (MPa s)	ρ (kg/m^3)
1	2.5	1	2.5	6450
cp (J/K)	T_M (K)			
600	272			

and temperature variations for these tests assuming different hypothetical values of h, showing that the increase of the coefficient h tends to cause less variations in stress-strain curves and in temperature values.

Another important aspect of the thermomechanical coupling modeling is that the temperature variation due to phase transformation does not occur when martensitic reorientation takes place. In order to observe this

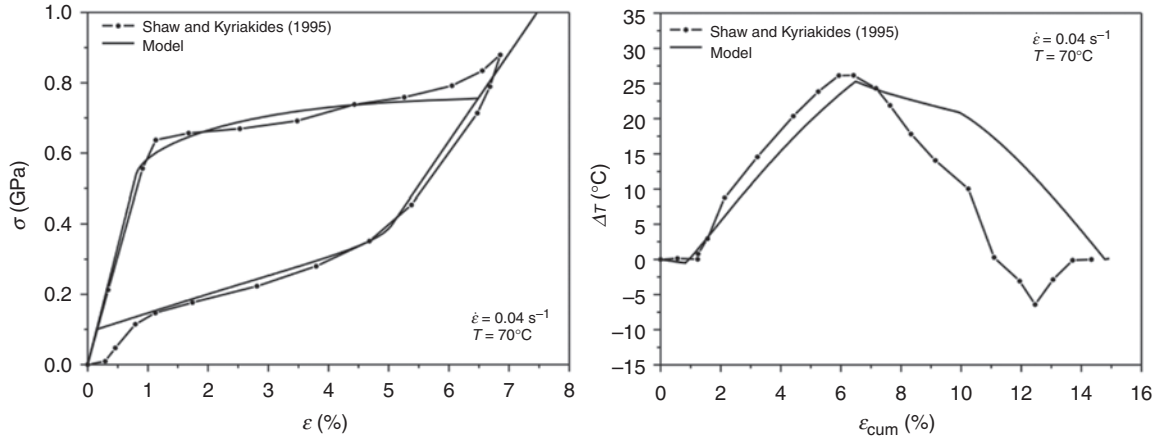

Figure 2. *Comparative results between experimental tests and model simulation in air with $\dot{\varepsilon} = 0.04\,s^{-1}$: stress–strain (left) and cumulative strain–temperature (right).*

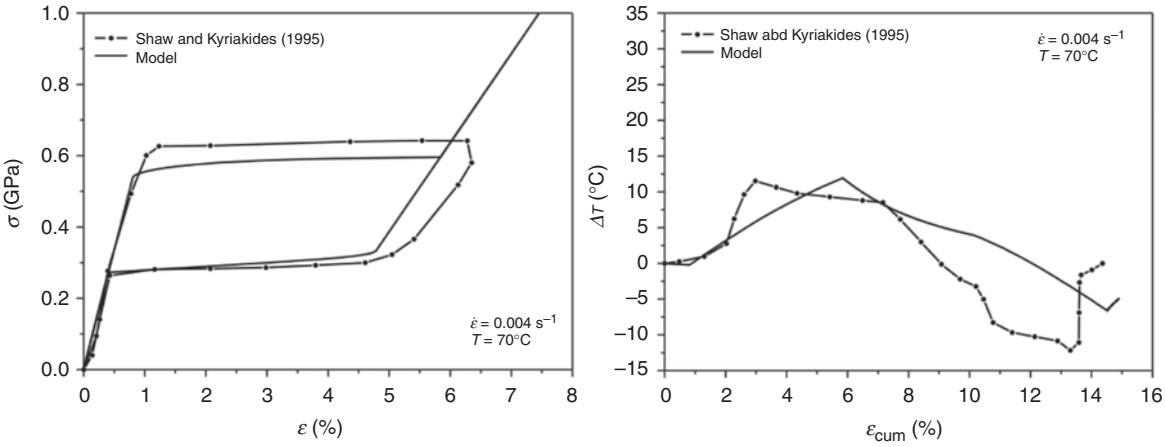

Figure 3. *Comparative results between experimental tests and model simulation in air with $\dot{\varepsilon} = 0.004\,s^{-1}$: stress–strain (left) and cumulative strain–temperature (right).*

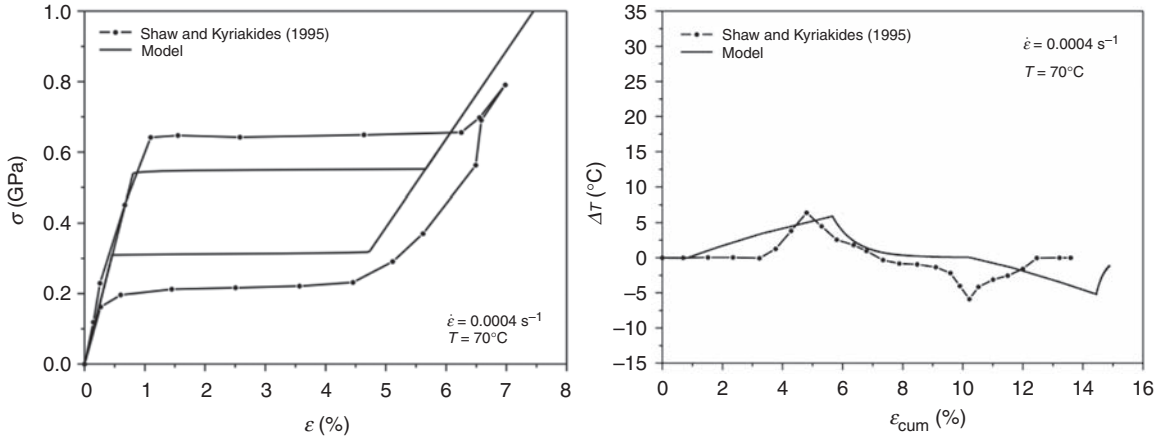

Figure 4. *Comparative results between experimental tests and model simulation in air with $\dot{\varepsilon} = 0.0004\,s^{-1}$: stress–strain (left) and cumulative strain–temperature (right).*

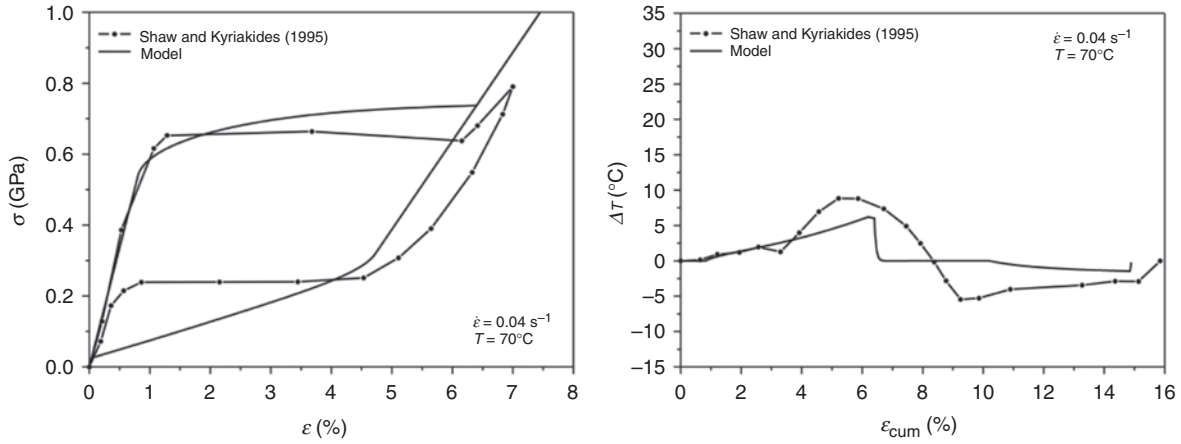

Figure 5. *Comparative results between experimental tests and model simulations in water with $\dot{\varepsilon} = 0.04\,s^{-1}$: stress–strain (left) and cumulative strain–temperature (right).*

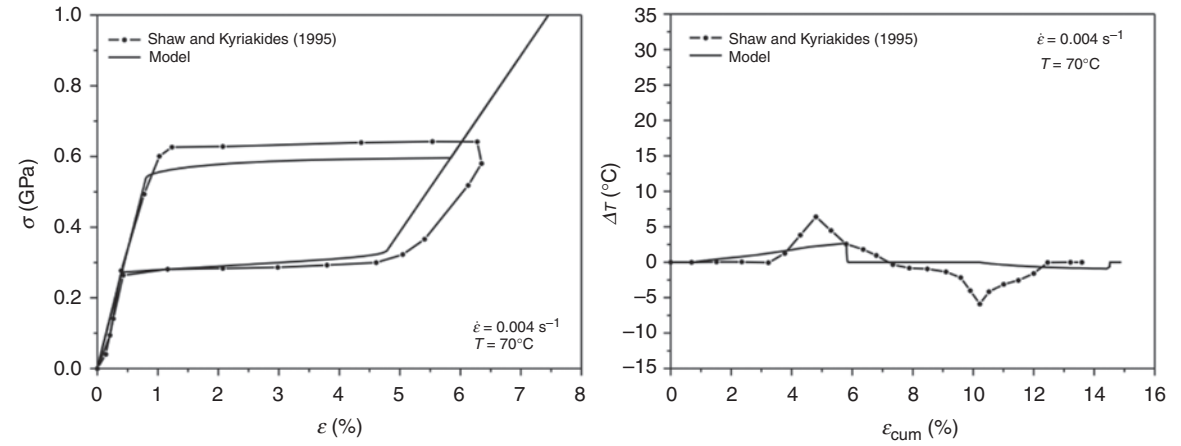

Figure 6. *Comparative results between experimental tests and model simulations in water with $\dot{\varepsilon} = 0.004\,s^{-1}$: stress–strain (left) and cumulative strain–temperature (right).*

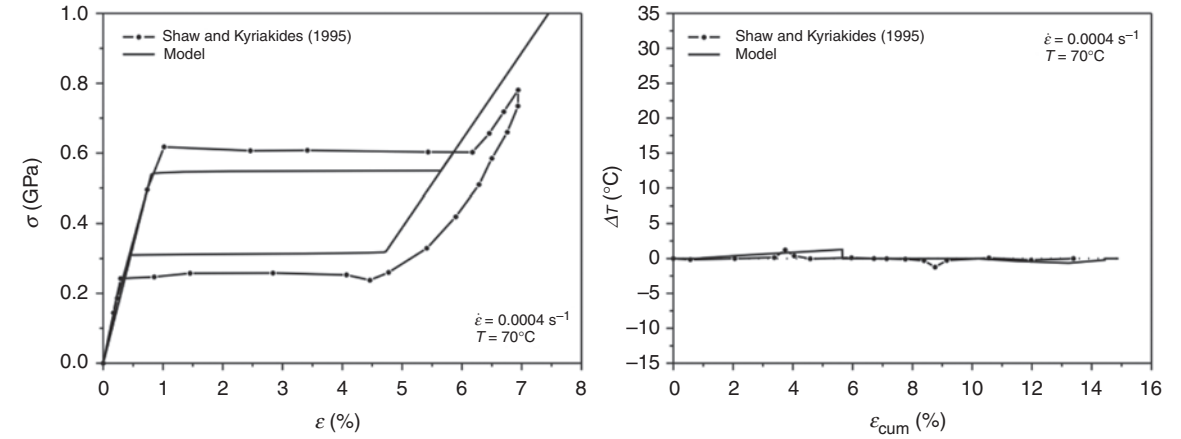

Figure 7. *Comparative results between experimental tests and model simulations in water with $\dot{\varepsilon} = 0.0004\,s^{-1}$: stress–strain (left) and cumulative strain–temperature (right).*

phenomenon, numerical tests are carried out simulating tensile tests with air as an environmental medium with different temperatures. The stress–strain curves together with temperature variations for these tests are presented in Figure 9 showing that temperature variations decrease as environmental temperature decreases and, therefore, martensitic reorientation is taking place instead of the austenite–martensite transformation. Note that

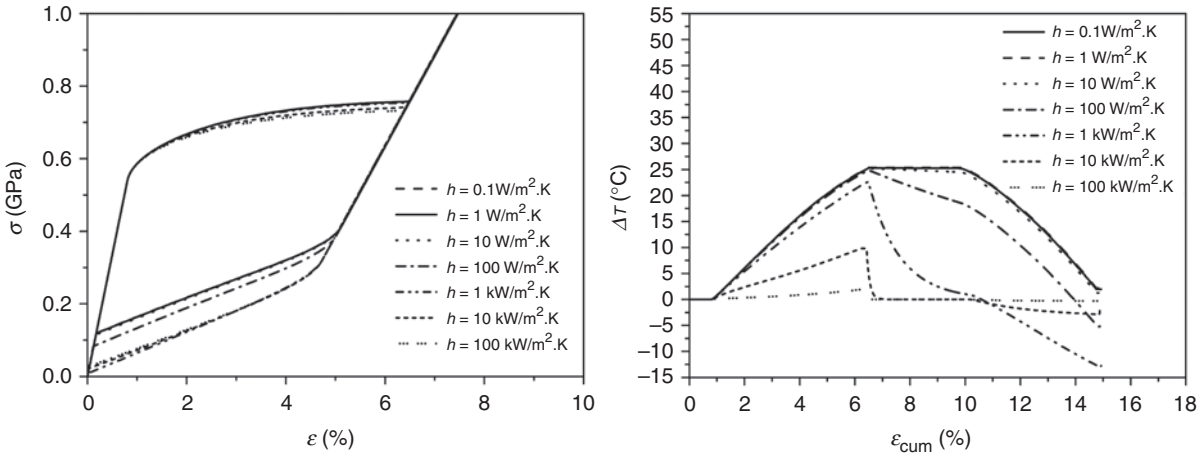

Figure 8. *Results for different h with $\dot{\varepsilon} = 0.04\,s^{-1}$: stress–strain (left) and cumulative strain–temperature (right).*

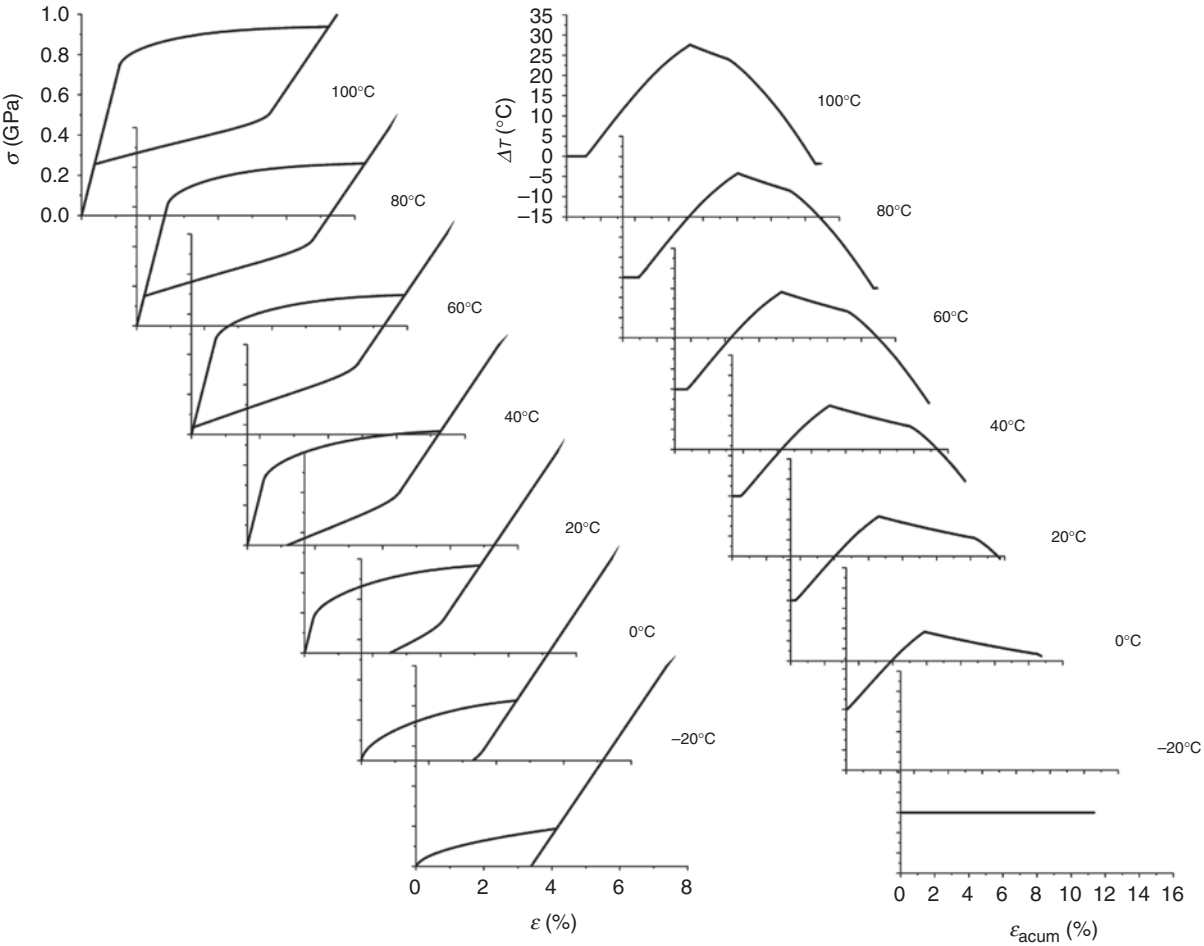

Figure 9. *Results for different temperatures in air with $\dot{\varepsilon} = 0.04\,s^{-1}$: stress–strain (left) and cumulative strain–temperature (right).*

martensitic reorientation occurs at $T_\infty = -20°C$. All other temperatures are assuming an austenitic initial state and, therefore, it is related to an austenite–martensite and its reverse phase transformation.

The SMA specimen is now subjected to different cyclic loadings considering different frequencies. Basically, 20 cycles are considered at a temperature $T_\infty = 70°C$ in air medium. Initially, let us consider that the mechanical loading is applied at 0.3 HZ representing a loading rate $\dot{\varepsilon} = 0.047\ s^{-1}$ (Figure 10). Under this condition, the SMA presents temperature oscillations due to phase transformation.

This frequency causes a proper balance between phase transformations and the heat convection and, as a consequence, the stress-strain curves present just a small variation from one cycle to another. By increasing the frequency to 1 HZ (Figure 11) at $\dot{\varepsilon} = 0.2\ s^{-1}$, the system response is significantly altered by temperature variations. Note that heat convection effect tends to decrease due to high frequency loadings. By changing the frequency to 30 HZ at $\dot{\varepsilon} - 1.08\ s^{-1}$ (Figure 12) the SMA behavior presents an even more

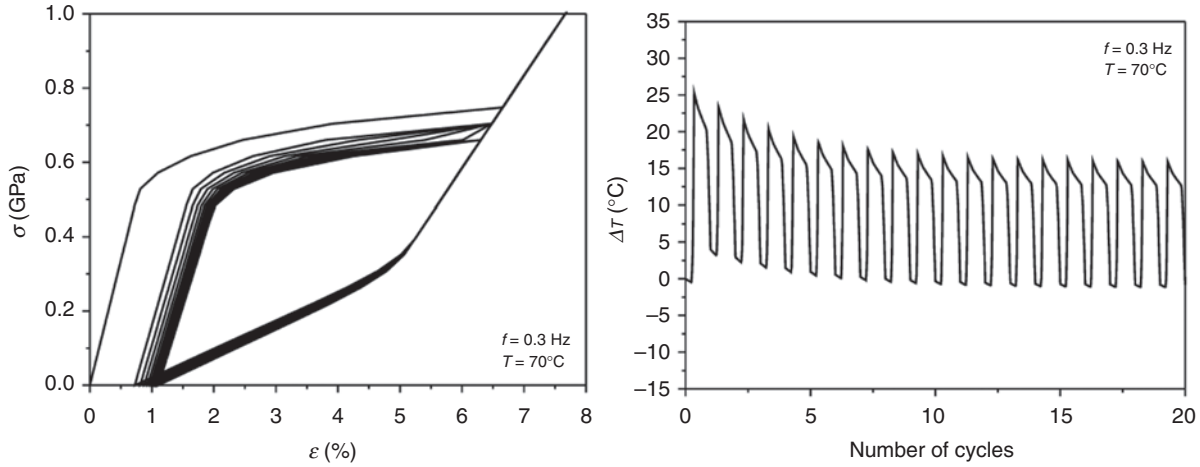

Figure 10. *Cyclic loading at 0.3 HZ: stress–strain (left) and temperature variation (right).*

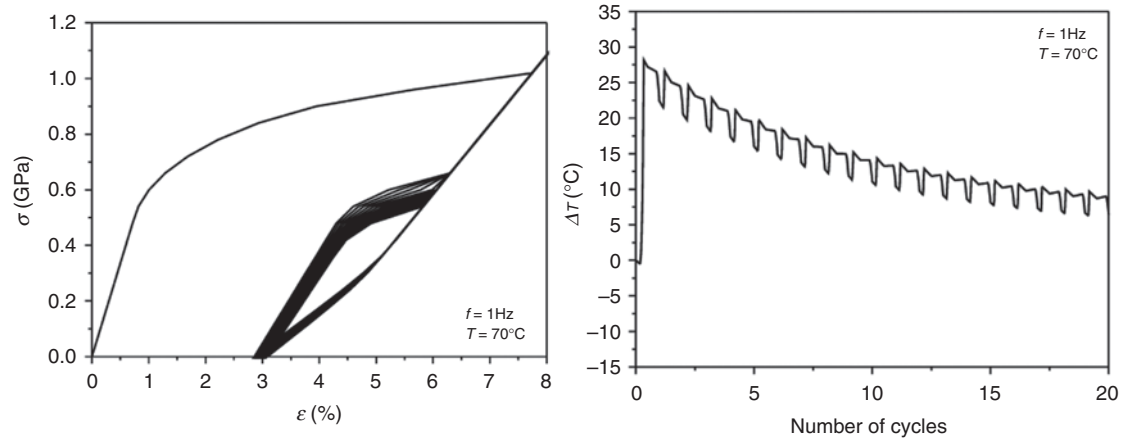

Figure 11. *Cyclic loading at 1 HZ: stress–strain (left) and temperature variation (right).*

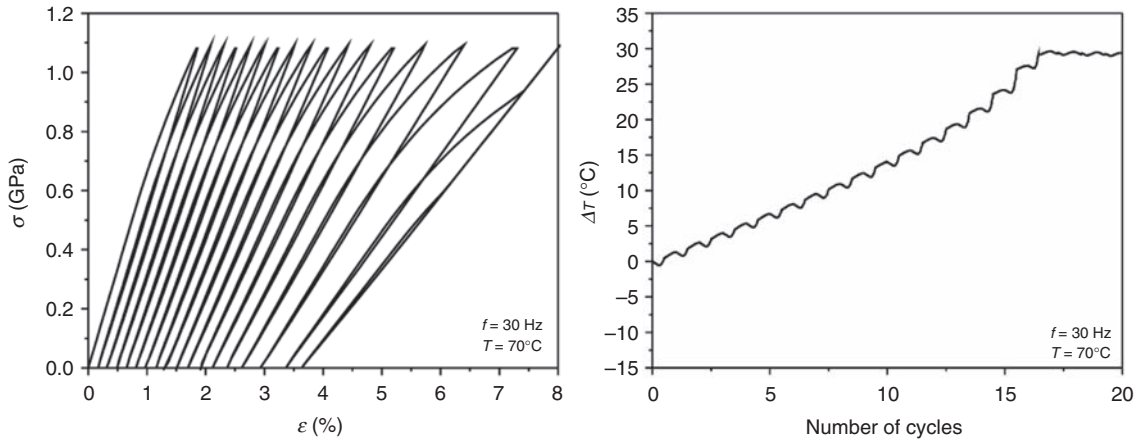

Figure 12. *Cyclic loading at 30 HZ: stress–strain (left) and temperature variation (right).*

evident influence and the hysteresis loop is completely modified.

Thermomechanical coupling may induce some tension–compression asymmetry since the increase of temperature causes a small difference on stress–strain curve. SMA parameters presented in Table 2 are used in order to match experimental tests made by Tobushi et al. (1998) for tensile tests, without asymmetry (Paiva et al., 2005). Figure 13 shows the SMA behavior for two different loading history: the first one considers tension and then compression (left side) while the second is the opposite situation (right side). Basically, due to different temperature variations that are related to thermal expansion terms, these two different loading histories can cause an asymmetric behavior in tension–compression response. Figure 14 shows the temperature evolution, showing differences that are responsible for the asymmetric behavior. Notice, however, that this asymmetry is just due to the thermomechanical coupling being not related to other mechanisms of SMA stress–strain asymmetry that causes smaller recoverable strain levels, higher critical transformation stress levels, and steeper transformation stress–strain slopes (Gall et al., 1999; Gall and Sehitoglu, 1999) that could also be captured by the proposed model as presented in Paiva et al. (2005).

Table 2. Model thermomechanical properties adjusted from experimental data (Tobushi et al., 1998).

Material properties				
E_A (GPa)	E_M (GPa)	a (MPa)	a_h	L_0 (MPa)
54	42	330	0.055	1
L (MPa)	L_0^A (MPa)	L^A (MPa)	Ω_A (MPa/K)	Ω_M (MPa/K)
41.5	0.63	185	0.74	0.17
η^L (MPa.s)	η^U (MPa.s)	η_3^L (MPa.s)	η_3^U (MPa.s)	ρ (kg/m^3)
1	2.7	1	2.7	6450
c_p (J/K)	T_M (K)			
600	291.4			

Let us now consider some simulations related to plastic behavior. The plasticity contributes to thermomechanical coupling effects and, therefore, let us treat some numerical simulations considering tensile tests of an SMA specimen in different temperatures, where model parameters are presented in Table 3. For high temperatures, there is a tendency that the material plastification occurs before the phase transformation. Hence, it is possible to compare the temperature variations due to phase transformation and plasticity. Basically, our tests treat three different environmental temperatures: 80°C (related to a martensitic state), 100°C (associated with an austenitic state), and 170°C (related to an austenitic state where plasticity occurs before the phase transformation due to the decrease of the yield limit caused by temperature). Figure 15 presents stress–strain curves of these tests while Figure 16 shows their temperature analysis, presenting the temperature variation against the total strain and the plastic strain. The mechanical

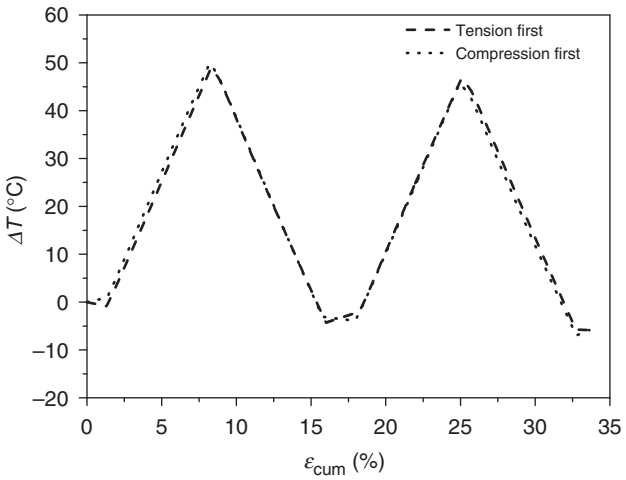

Figure 14. *Temperature-accumulated strain curves for two different paths: tension first and compression first loads at* $\dot{\varepsilon} = 0.04\ s^{-1}$.

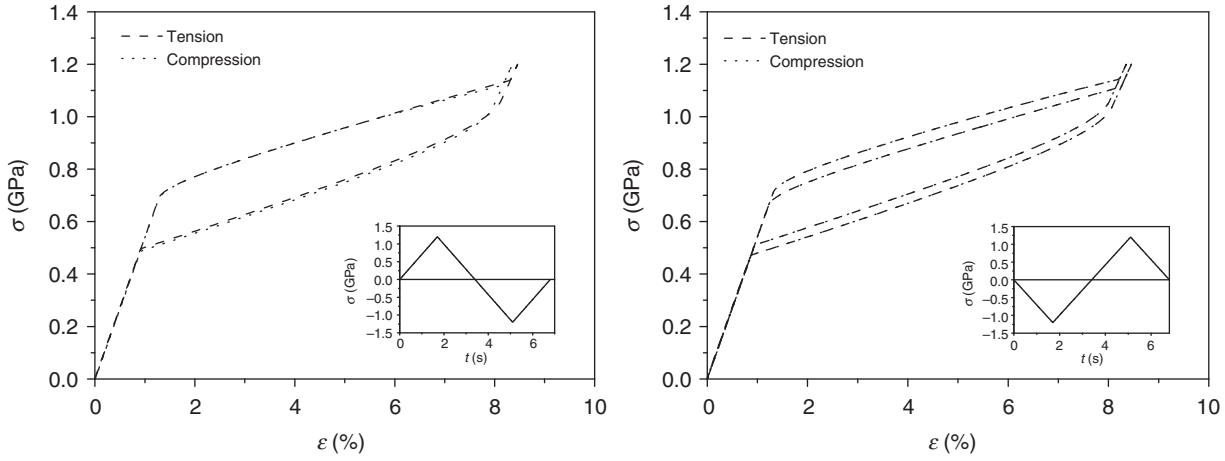

Figure 13. *Stress–strain curves for two different paths of tension–compression loads at* $\dot{\varepsilon} = 0.04\ s^{-1}$*: tension first (left) and compression first (right).*

loading of all three cases is such that causes plastic deformation. When $T_\infty = 80^\circ$C there is a martensitic reorientation before the plastification. The temperature change occurs just due to the plastification since the martensitic reorientation does not produce temperature variations. When, $T_\infty = 100^\circ$C, an austenite–martensite transformation takes place before the plastification. Under this condition, there are two sources of temperature variations: phase transformation and plastification. Therefore, this situation has greater variations when compared with the other situations. Finally, when, $T_\infty = 170^\circ$C, the plastification occurs before the phase transformation has taken place. Temperature variations are, therefore, only due to the plasticity.

Table 3. Model thermomechanical properties.

Material properties				
E_A (GPa)	E_M (GPa)	a (MPa)	a_h	L_0 (MPa)
70	18	225	0.055	4
L (MPa)	L_0^A(MPa)	L^A (MPa)	Ω_A (MPa/K)	Ω_M (MPa/K)
10	1	120	0.74	0.17
η^L (MPa.s)	η^U (MPa.s)	η_3^L (MPa.s)	η_3^U (MPa.s)	ρ (kg/m^3)
1	2.5	1	2.5	6450
c_p (J/K)	T_M (K)	H_A (GPa)	H_M (GPa)	K_A (GPa)
600	363	0.4	0.2	0.1
K_M (GPa)	σ_Y^{Aj} (GPa)	σ_Y^{Aj} (GPa)	σ_Y^M (GPa)	
0.1	0.98	0.65	0.75	

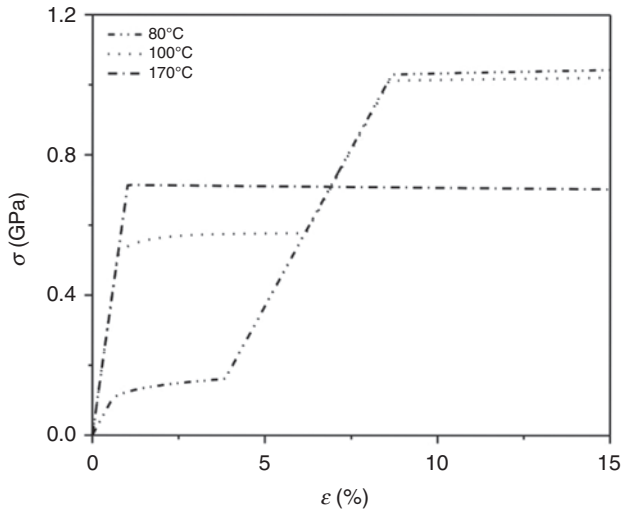

Figure 15. *Stress–strain curves for three different temperatures at $\dot{\varepsilon} = 0.04\,s^{-1}$: including phase transformation and plasticity effects.*

CONCLUSIONS

This article discusses a phenomenological model to describe the SMA rate-dependent behavior by considering thermomechanical coupling. The model is built upon a previous version developed by Paiva et al. (2005) incorporating the thermomechanical coupling in energy equation. Numerical simulations establish a comparison between numerical and experimental results available in literature showing a close agreement for different loading rates and environmental media. After the model verification, some numerical tests are carried out. The cyclic response of an SMA specimen is investigated showing the importance of the balance between loading rate and heat convection. Moreover, some interesting situations may be observed due to thermomechanical coupling effects as a tension–compression asymmetry. The influence of plasticity is also treated showing its importance in the temperature variations. We can conclude that the model is capable to capture the general thermomechanical behavior of SMAs, proper describing the rate-dependent characteristics and the thermomechanical coupling aspects.

ACKNOWLEDGMENT

The authors acknowledge the support of the Brazilian Research Councils CNPq, FAPERJ and ANP.

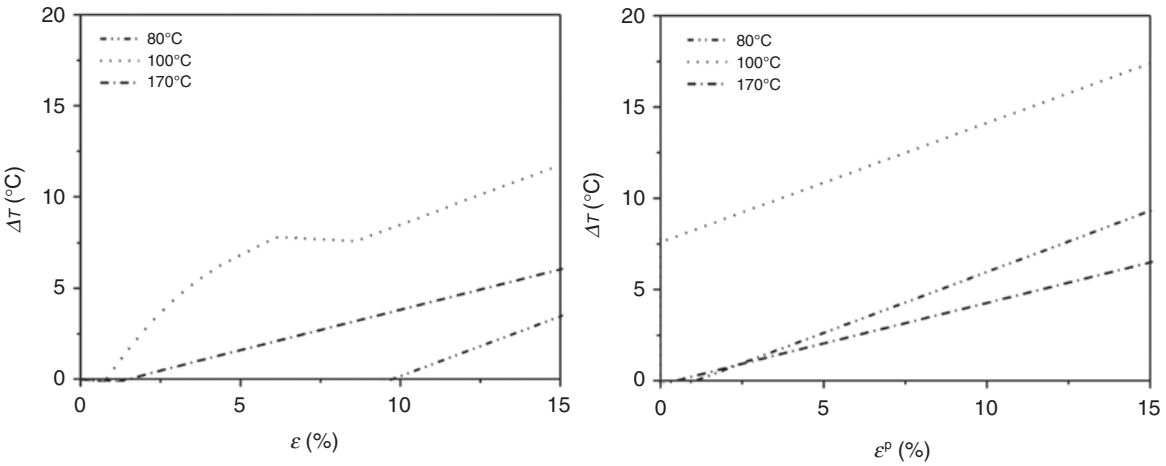

Figure 16. *Temperature–strain curves for three different temperatures (left) and temperature–plastic strain (right).*

REFERENCES

Auricchio, F., Fugazza, D. and DesRoches, R. 2006. "Numerical and Experimental Evaluation of the Damping Properties of Shape-memory Alloys," *Journal of Engineering Materials and Technology – ASME*, 128:312–319.

Auricchio, F., Reali, A. and Stefanelli, U. 2007. "A Three-dimensional Model Describing Stress-induced Solid Phase Transformation with Permanent Inelasticity," *International Journal of Plasticity*, 23:207–226.

Auricchio, F., Taylor, R.L. and Lubliner, J. 1997. "Shape-memory Alloys: Macromodeling and Numerical Simulations of the Superelastic Behavior," *Computer Methods in Applied Mechanics and Engineering*, 146(3–4):281–312.

Baêta-Neves, A.P., Savi, M.A. and Pacheco, P.M.C.L. 2004. "On the Fremond's Constitutive Model for Shape Memory Alloys," *Mechanics Research Communications*, 31(6):677–688.

Bernardini, D. and Pence, T.J. 2002. "Models for One-variant Shape Memory Materials Based on Dissipation Functions," *International Journal of Non-linear Mechanics*, 37(8):1299–1317.

Bernardini, D. and Pence, T.J. 2005. "Uniaxial Modeling of Multivariant Shape-memory Materials with Internal Sublooping Using Dissipation Functions," *Meccanica*, 40(4–6):339–364.

Bo, Z.H. and Lagoudas, D.C. 1999. "Thermomechanical Modeling of Polycrystalline SMAs Under Cyclic Loading. Part III: Evolution of Plastic Strains and Two-way Shape Memory Effect," *International Journal of Engineering Science*, 37(9): 1175–1203.

Boyd, J.G. and Lagoudas, D.C. 1996. "Thermodynamic Constitutive Model for the Shape Memory Materials – Part I: The Monolithic Shape Memory Alloys," *International Journal of Plasticity*, 12(6):805–842.

Brinson, L.C. 1993. "One Dimensional Constitutive Behavior of Shape Memory Alloys: Themomechanical Derivation with Non-constant Material Functions and Redefined Martensite Internal Variable," *Journal of Intelligent Material Systems and Structures*, 4:229–242.

Chang, B.C., Shaw, J.A. and Iadicola, M.A. 2006. "Thermodynamics of Shape Memory Alloy Wire: Modeling, Experiments, and Application," *Continuum Mechanics and Thermodynamics*, 18(1–2): 83–118.

Dayananda, G.N. and Subba Rao, M. 2008. "Effect of Strain Rate on Properties of Superelastic NiTi Thin Wires," *Materials Science and Engineering A*, 486:96–103.

Davis, B., Turner, T.L. and Seelecke, S. 2008. "Measurement and Prediction of the Thermomechanical Response of Shape Memory Alloy Hybrid Composite Beams," *Journal of Intelligent Material Systems and Structures*, 19(2):129–143.

Fremond, M. 1987. "Matériaux à Mémoire de Forme," *Comptes Rendus des séances l'Academie des Sciences, Paris, Tome 34*, 7:239–244.

Fremond, M. 1996. *Shape Memory Alloy: A Thermomechanical Macroscopic Theory,* CISM Courses and Lectures, Springer Verlag, New York.

Gall, K., Sehitoglu, H., Chumlyakov, Y.I. and Kireeva, I.V. 1999. "Tension-compression Asymmetry of the Stress-strain Response in Aged Single Crystal and Polycrystalline NiTi," *Acta Materialia*, 47(4):1203–1217.

Gall, K. and Sehitoglu, H. 1999. "The Role of Texture in Tension-compression Asymmetry in Polycrystalline NiTi," *International Journal of Plasticity*, 15:69–92.

Grabe, C. and Bruhns, O.T. 2008. "On the Viscous and Strain Rate Dependent Behavior of Polycrystalline NiTi," *International Journal of Solids and Structures*, 45:1876–1895.

Heintze, O. and Seelecke, S. 2008. "A Coupled Thermomechanical Model for Shape Memory Alloys - From Single Crystal to Polycrystal," *Materials Science and Engineering A - Structural Materials Properties Microstructure and Processing*, 481:389–394.

Iadicola, M.A. and Shaw, J.A. 2004. "Rate and Thermal Sensitivities of Unstable Transformation Behavior in a Shape Memory Alloy," *International Journal of Plasticity*, 20:577–605.

Iadicola, M.A. and Shaw, J.A. 2007. "An Experimental Method to Measure Initiation Events During Unstable Stress-induced Martensitic Transformation in a Shape Memory Alloy Wire," *Smart Materials and Structures*, 16:S155–S169.

Incropera, F.P. and Dewitt, D.P. 2001. *Fundamentals of Heat and Mass Transfer*, 5th edn, John Wiley & Sons, Canada.

Kadkhodaei, M., Rajapakse, R.K.N.D., Mahzoon, M. and Salimi, M. 2007. "Modeling of the Cyclic Thermomechanical Response of SMA Wires at Different Strain Rates," *Smart Materials and Structures*, 16:2091–2101.

Lemaitre, J. and Chaboche, J.-L. 1990. *Mechanics of Solid Materials*, Cambridge University Press, London.

Liang, C. and Rogers, C.A. 1990. "1D Thermomechanical Constitutive Relations for Shape Memory Materials," *Journal of Intelligent Material Systems and Structures*, 1:207–234.

Paiva, A., Savi, M.A., Braga, A.M.B. and Pacheco, P.M.C.L. 2005. "A Constitutive Model for Shape Memory Alloys Considering Tensile-compressive Asymmetry and Plasticity," *International Journal of Solids and Structures*, 42(11–12):3439–3457.

Paiva, A. and Savi, M.A. 2006. "An Overview of Constitutive Models for Shape Memory Alloys," *Mathematical Problems in Engineering*, 2006:1–30.

Prahlad, H. and Chopra, I. 2001. "Comparative Evaluation of Shape Memory Alloy Constitutive Models with Experimental Data," *Journal of Intelligent Material Systems and Structures*, 12(6):383–395.

Prahlad, H. and Chopra, I. 2003. "Development of a Strain-rate Dependent Model for Uniaxial Loading of SMA Wires," *Journal of Intelligent Material Systems and Structures*, 14(7):429–442.

Rockafellar, R.T. 1970. *Convex Analysis*, Princeton Press, Princeton, New Jersey.

Savi, M.A., Paiva, A., Baêta-Neves, A.P. and Pacheco, P.M.C.L. 2002. "Phenomenological Modeling and Numerical Simulation of Shape Memory Alloys: A Thermo-plastic-phase Transformation Coupled Model," *Journal of Intelligent Material Systems and Structures*, 13(5):261–273.

Savi, M.A. and Paiva, A. 2005. "Describing Internal Subloops due to Incomplete Phase Transformations in Shape Memory Alloys," *Archive of Applied Mechanics*, 74(9):637–647.

Shaw, J.A. and Kyriakides, S. 1995. "Thermomechanical Aspects of Ni-Ti," *Journal of the Mechanics and Physics of Solids*, 43(8):1243–1281.

Tanaka, K. and Nagaki, S. 1982. "Thermomechanical Description of Materials with Internal Variables in the Process of Phase Transformation," *Ingenieur Archiv*, 51:287–299.

Thiebaud, F., Lexcellent, C., Collet, M. and Foltete, E. 2007. "Implementation of a Model Taking into Account the Asymmetry Between Tension and Compression, the Temperature Effects in a Finite Element Code for Shape Memory Alloys Structures Calculations," *Computational Materials Science*, 41:208–221.

Tobushi, H., Shimeno, Y., Hachisuka, T. and Tanaka, K. 1998. "Influence of Strain Rate on Superelastic Properties of TiNi Shape Memory Alloy," *Mechanics of Materials*, 30(2):141–150.

Yoon, S.H. 2008. "Experimental Investigation of Thermo-mechanical Behaviors in Ni-Ti Shape Memory Alloy," *Journal of Intelligent Material Systems and Structures*, 19(3):283–289.

Zhu, S. and Zhang, Y. 2007. "A Thermomechanical Constitutive Model for Superelastic SMA Wire with Strain-rate Dependence," *Smart Material and Structures*, 16:1696–1707.

Ziólkowski, A. 2007. "Three-dimensional Phenomenological Thermodynamic Model of Pseudoelasticity of Shape Memory Alloys at Finite Strains," *Continuum Mechanics and Thermodynamics*, 19:379–398.